Photoelectron spectra in an autoionization system interacting with a neighboring atom

Jan Peřina Jr.,[1,*] Antonín Lukš,[2] Wieslaw Leoński,[3] and Vlasta Peřinová[2]

[1]*Joint Laboratory of Optics, Institute of Physics of ASCR, 17 Listopadu 50a, CZ-772 07 Olomouc, Czech Republic*

[2]*Joint Laboratory of Optics, Palacký University, RCPTM, 17 Listopadu 12, CZ-771 46 Olomouc, Czech Republic*

[3]*Quantum Optics and Engineering Division, Institute of Physics, University of Zielona Góra, Prof. Z. Szafrana 4a, PL-65-516 Zielona Góra, Poland*

(Received 17 March 2011; published 31 May 2011)

Photoelectron ionization spectra of an autoionization system with one discrete level interacting with a neighbor two-level atom are discussed. The formula for long-time ionization spectra is derived. According to this formula, the spectra can be composed of up to eight peaks. Moreover, the Fano-like zeros for weak optical pumping are identified in these spectra. The conditional ionization spectra depending on the state of the neighbor atom exhibit oscillations at the Rabi frequency. Dynamical spectral zeros occurring once per the Rabi period are revealed in these spectra.

DOI: 10.1103/PhysRevA.83.053430 PACS number(s): 32.80.−t, 33.80.Eh, 34.20.−b

I. INTRODUCTION

The problem of ionization of an atom with discrete autoionizing levels has been addressed many times under various conditions since the pioneering work by Fano [1] appeared. In his contribution, Fano explained the existence of unpopulated frequencies in the continuum of ionized states by diagonalizing the appropriate Hamiltonian. This effect occurs as a consequence of destructive interference of two quantum ionization paths. This phenomenon occurring at specific frequencies (or for given ionization states) is spoken of as the presence of "Fano zeros." Moreover, there might occur a strong narrowing of spectral peaks in the vicinity of such frequencies by virtue of strong interference. This effect is sometimes referred to as the "confluence of bound-free coherences" [2]. These effects can be degraded to a certain extent by, for example, spontaneous emission of radiation [3–5], a finite pump laser bandwidth [6], and collisions [5]. In general, there exist n Fano zeros in an autoionization system with n discrete autoionizing levels [1,7]. Generalizations including several mutually noninteracting continua have also been given [1,8]. The presence of autoionizing levels also influences ionization dynamics under strong laser pumping [9]. Experimental observation of Fano spectral zeros has been reported, for example, in [10]. The existence of discrete levels in autoionization systems can lead to transparency for ultrashort pulses [11] or slowing-down of propagating light [12]. The dynamics of ionization can even be influenced by Zeno or anti-Zeno effects [13]. A generalization to low-light quantum optical fields including Fock coherent or squeezed states has also been given [14,15] and it revealed additional interferences in photoelectron ionization spectra stemming from the discrete energies of quantized optical fields. The ionization quantum-path interference effects studied play an important role in spectroscopy in explaining asymmetric spectral profiles [16]. Similar quantum interference effects can be found in many other fields of physics, using both mass particles and photons. Among others, semiconductor heterostructures or photonic wave guides can be mentioned [17]. An extended list of references dealing with autoionization can be found in [5,7], and [18].

In this work we continue the investigation of the influence of a neighbor atom on an ionization system and its long-time photoelectron ionization spectra. The influence is assumed to have the form of energy transfer caused, for example, by dipole-dipole interaction. Compared to [19], we additionally assume one discrete bound (autoionizing) state present in the ionization system. Similarly to [19], the neighbor atom is modeled as a two-level system that undergoes Rabi oscillations in a stationary optical field. These oscillations significantly influence conditional photoelectron spectra of the autoionization system. In these spectra, so-called dynamical zeros occurring once per Rabi period [19] have been found. Frequencies in photoelectron ionization spectra corresponding to both Fano-like zeros (for weak optical pumping) and dynamical zeros are studied using both analytical and numerical approaches. Molecular condensates [20] as well as systems of quantum dots or other semiconductor heterostructures [17] are suitable candidates for verification of the results obtained.

The paper is organized as follows. Section II reports the model Hamiltonian, solution of the corresponding Schrödinger equation, and formulas for photoelectron ionization spectra. These spectra in their long-time limit are discussed in Sec. III. The frequencies of Fano-like zeros in the spectra are analyzed in Sec. IV using the method of canonical transformation. Section V is devoted to dynamical zeros. Conclusions are drawn in Sec. VI. Formulas giving the frequencies of poles of the Lorentzian curves constituting the photoelectron ionization spectra are given in Appendix A. A method for the determination of frequencies of Fano as well as dynamical zeros is developed in Appendix B.

II. QUANTUM MODEL AND ITS PHOTOELECTRON IONIZATION SPECTRA

The considered ionization system (atom, molecule), with one autoionizing level, is assumed to interact with a neighbor two-level atom (molecule) by dipole-dipole interaction (for the scheme, see Fig. 1). Both the ionization system and the neighbor atom are under the influence of a stationary optical field. The Hamiltonian $\hat{H}_{\mathrm{a-i}}$ of ionization system b with

*perinaj@prfnw.upol.cz

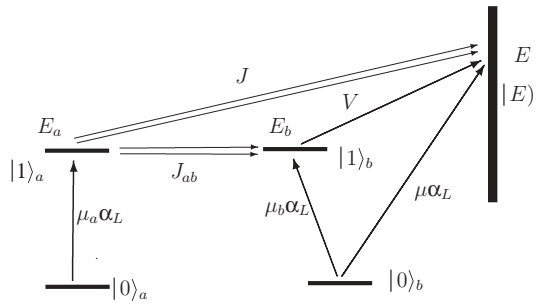

FIG. 1. Scheme of autoionization system b interacting with the two-level atom a. State $|1\rangle_a$ means an excited state of atom a with energy E_a, $|1\rangle_b$ stands for an excited bound state of autoionization system b with energy E_b, and $|E)$ is a free state inside the continuum at atom b with energy E. μ_a, μ_b, and μ denote the dipole moments between the ground states $|0\rangle_a$ and $|0\rangle_b$ and the corresponding excited states, α_L stands for the pumping amplitude, V describes the Coulomb configurational coupling between state $|1\rangle_b$ and state $|E)$, and J [J_{ab}] refers to the dipole-dipole interaction between state$|1\rangle_a$ and state $|E)$ [$|1\rangle_b$]. Double arrows indicate that two electrons at atoms a and b participate in the interaction (energy transfer).

one autoionizing level can be written in the form ($\hbar = 1$ is assumed [21])

$$\begin{aligned}\hat{H}_{\mathrm{a-i}} = {} & E_b|1\rangle_{bb}\langle 1| + \int dE\, E|E)(E| \\ & + \int dE(V|E)_b\langle 1| + \mathrm{H.c.}) \\ & + [\mu_b\alpha_L \exp(-iE_Lt)|1\rangle_{bb}\langle 0| + \mathrm{H.c.}] \\ & + \int dE[\mu\alpha_L \exp(-iE_Lt)|E)_b\langle 0| + \mathrm{H.c.}]. \end{aligned} \quad (1)$$

In Eq. (1), the symbol E_b means the excitation energy from the ground state $|0\rangle_b$ into the excited bound state $|1\rangle_b$ of atom b. The continuum of autoionization system b is formed by the states $|E)$ with their energies E. The coupling constant V describes the Coulomb configuration interaction between state $|1\rangle_b$ and state $|E)$ inside the continuum. The dipole moments μ_b and μ characterize the optical excitation of the corresponding states; α_L means an optical-field amplitude oscillating at frequency E_L. H.c. stands for the Hermitian conjugated term.

A neighbor two-level atom a interacting with the optical field through the dipole moment μ_a is described by the Jaynes-Cummings Hamiltonian $\hat{H}_{t-a}$:

$$\hat{H}_{t-a} = E_a|1\rangle_{aa}\langle 1| + [\mu_a\alpha_L \exp(-iE_Lt)|1\rangle_{aa}\langle 0| + \mathrm{H.c.}]. \quad (2)$$

The energy E_a of the excited bound state $|1\rangle_a$ of atom a is measured relative to the energy of the ground state $|0\rangle_a$. The ground states of atoms a and b are assumed to have the same energy, which is chosen to be 0.

The energy transfer [20] caused by the dipole-dipole interaction between the two-level atom a and the autoionizing system b is characterized by the Hamiltonian $\hat{H}^e_{\mathrm{trans}}$:

$$\begin{aligned}\hat{H}^e_{\mathrm{trans}} = {} & [J_{ab}|1\rangle_{bb}\langle 0||0\rangle_{aa}\langle 1| + \mathrm{H.c.}] \\ & + \int dE[J|E)_b\langle 0||0\rangle_{aa}\langle 1| + \mathrm{H.c.}]. \end{aligned} \quad (3)$$

In this interaction, one electron looses its energy when returning from the excited state into the ground state, whereas the other one absorbs this energy and moves from the ground state into its own excited state. The constants J_{ab} and J quantify the strength of this interaction.

A general quantum state of two electrons in atoms a and b can be written in the following form appropriate to the rotating frame:

$$\begin{aligned}|\psi\rangle(t) = {} & c_{00}(t)|0\rangle_a|0\rangle_b + c_{10}(t)|1\rangle_a|0\rangle_b \\ & + c_{01}(t)|0\rangle_a|1\rangle_b + c_{11}(t)|1\rangle_a|1\rangle_b \\ & + \int dE\, d_0(E,t)|0\rangle_a|E) \\ & + \int dE\, d_1(E,t)|1\rangle_a|E). \end{aligned} \quad (4)$$

The time-dependent coefficients c_{00}, c_{10}, c_{01}, c_{11}, $d_0(E)$, and $d_1(E)$ characterize state $|\psi\rangle$ at an arbitrary time.

The Schrödinger equation with the Hamiltonian $\hat{H}_{a-i} + \hat{H}_{t-a} + \hat{H}^e_{\mathrm{trans}}$ can be written as a system of differential equations for the coefficients of decomposition written in Eq. (4):

$$i\frac{d}{dt}\begin{bmatrix}\mathbf{c^e(t)}\\ \mathbf{d}(E,t)\end{bmatrix} = \begin{bmatrix}\mathbf{A^e} & \mathbf{B^e}\int dE\\ \mathbf{B^{e\dagger}} & \mathbf{K}(E)\end{bmatrix}\begin{bmatrix}\mathbf{c^e(t)}\\ \mathbf{d}(E,t)\end{bmatrix}. \quad (5)$$

The symbol † denotes the Hermitian conjugation. The vectors $\mathbf{c^e}$ and $\mathbf{d}$ and the matrices $\mathbf{A^e}$, $\mathbf{B^e}$, and $\mathbf{K}$ introduced in Eq. (6) can be derived in the form

$$\mathbf{c^e}(t) = \begin{bmatrix}c_{00}(t)\\ c_{10}(t)\\ c_{01}(t)\\ c_{11}(t)\end{bmatrix}, \quad \mathbf{d}(E,t) = \begin{bmatrix}d_0(E,t)\\ d_1(E,t)\end{bmatrix}, \quad (6)$$

$$\mathbf{A^e} = \begin{bmatrix}0 & \mu_a^*\alpha_L^* & \mu_b^*\alpha_L^* & 0\\ \mu_a\alpha_L & \Delta E_a & J_{ab}^* & \mu_b^*\alpha_L^*\\ \mu_b\alpha_L & J_{ab} & \Delta E_b & \mu_a^*\alpha_L^*\\ 0 & \mu_b\alpha_L & \mu_a\alpha_L & \Delta E_a + \Delta E_b\end{bmatrix}, \quad (7)$$

$$\mathbf{B^e} = \begin{bmatrix}\mu^*\alpha_L^* & 0\\ J^* & \mu^*\alpha_L^*\\ V^* & 0\\ 0 & V^*\end{bmatrix}, \quad (8)$$

$$\mathbf{K}(E) = \begin{bmatrix}E - E_L & \mu_a^*\alpha_L^*\\ \mu_a\alpha_L & E - E_L + \Delta E_a\end{bmatrix}; \quad (9)$$

$\Delta E_a = E_a - E_L$ and $\Delta E_b = E_b - E_L$. As the electrons remain inside the system during the evolution, the norm of state $|\psi\rangle$ is preserved:

$$\sum_{j,k=0}^{1} |c_{jk}(t)|^2 + \sum_{j=0}^{1} \int dE |d_j(E,t)|^2 = 1. \tag{10}$$

The system of differential equations (6) can be solved using the Laplace-transform method (for details, see [19]). The coefficients $d_0(E,t)$ and $d_1(E,t)$ of the solution then give the amplitude photoelectron ionization spectra of atom b conditioned by the presence of atom a in the ground and excited states, respectively. It can be shown that, in the solution, there exist two prominent frequencies ξ_1 and ξ_2 characterizing oscillations of the neighbor atom a:

$$\begin{aligned} \xi_{1,2} &= E_L - \frac{\Delta E_a \pm \delta\xi}{2}, \\ \delta\xi &= \sqrt{(\Delta E_a)^2 + 4|\mu_a \alpha_L|^2}. \end{aligned} \tag{11}$$

The solution for coefficients $\mathbf{d}(E,t)$ can be derived as follows [19]:

$$\mathbf{d}(E,t) = \mathbf{d}^{\xi_1}(E,t) + \mathbf{d}^{\xi_2}(E,t), \tag{12}$$

$$\mathbf{d}^{\xi_j}(E,t) = i\mathbf{K_j}\mathbf{B}^{\mathbf{e}\dagger}\mathbf{P}^{\mathbf{e}}\mathbf{U}^{\mathbf{e}}_{\mathbf{k}}(E,t)\mathbf{P}^{\mathbf{e}-\mathbf{1}}\mathbf{c}^{\mathbf{e}}(0), \quad j = 1,2. \tag{13}$$

The elements of the diagonal evolution matrices $\mathbf{U}^{\mathbf{e}}_{\mathbf{k}}$, $k = 1,2$, in Eq. (13) are given as

$$\begin{aligned} \left[\mathbf{U}^{\mathbf{e}}_{\mathbf{k}}\right]_{jl}(E,t) = \frac{i\delta_{jl}}{E - \Lambda_{M^e,j} - \xi_k} &[\exp[i(\xi_k - E)t] \\ &- \exp(-i\Lambda_{M^e,j}t)], \end{aligned} \tag{14}$$

δ_{jk} being the Kronecker symbol. The symbols $\Lambda_{M^e,j}$ denote eigenvalues of the evolution matrix $\mathbf{M^e}$, $\mathbf{M^e} = \mathbf{A^e} - i\pi\mathbf{B^e}\mathbf{B^{e\dagger}}$. The eigenvectors of matrix $\mathbf{M^e}$ then form the columns of matrix $\mathbf{P^e}$ introduced in Eq. (13). The matrices $\mathbf{K_k}$ occurring in Eq. (13) take the form

$$\mathbf{K_k} = \frac{(-1)^k}{\delta\xi} \begin{bmatrix} E_a + \xi_k & -\mu_a^* \alpha_L^* \\ -\mu_a \alpha_L & E_L + \xi_k \end{bmatrix}. \tag{15}$$

The vector $\mathbf{c^e}(0)$ in Eq. (13) gives the initial conditions. We assume here that electrons in both the two-level atom a and the autoionizing system b are initially in their ground states, that is, $\mathbf{c^e}(0) = (1,0,0,0)$.

In deriving the long-time photoelectron ionization spectra, the long-time form of the evolution matrices $\mathbf{U}^{\mathbf{e}}_{\mathbf{k}}$ defined in Eq. (14) is needed:

$$\left[\mathbf{U}^{\mathbf{e,lt}}_{\mathbf{k}}\right]_{jl}(E,t) = \frac{i\delta_{jl}\exp[i(\xi_k - E)t]}{E - \Lambda_{M^e,j} - \xi_k}. \tag{16}$$

We note that formula (16) is valid for times t obeying $t \gg 1/|\mathrm{Im}\{\Lambda_{M^e,j}\}|$ for $j = 1,\ldots,4$; Im indicates the imaginary part. The long-time form of evolution matrices $\mathbf{U}^{\mathbf{e,lt}}_{\mathbf{1}}$ and $\mathbf{U}^{\mathbf{e,lt}}_{\mathbf{2}}$ shows that oscillations at the Rabi frequency $\delta\xi = \xi_1 - \xi_2$ occur in the intensity photoelectron ionization spectra I^{lt}_j, $I^{\mathrm{lt}}_j(E) \equiv |d^{\mathrm{lt}}_j(E)|^2$. A detailed analysis has shown [19] that the long-time intensity spectra I^{lt}_0 and I^{lt}_1 can be expressed in a specific form:

$$\begin{aligned} I^{\mathrm{lt}}_0(E,t) &= I^{\mathrm{st}}_0(E) + I^{\mathrm{osc}}(E)\cos[\delta\xi t + \varphi(E)], \\ I^{\mathrm{lt}}_1(E,t) &= I^{\mathrm{st}}_1(E) - I^{\mathrm{osc}}(E)\cos[\delta\xi t + \varphi(E)]. \end{aligned} \tag{17}$$

The intensities I^{st}_0 and I^{st}_1 denote the steady-state parts of the corresponding spectra, whereas the intensity I^{osc} describes the magnitude of harmonic oscillations between spectrum I^{lt}_0 and spectrum I^{lt}_1. The symbol φ stands for a spectrally dependent phase. These temporal oscillations at the Rabi frequency in the conditional long-time photoelectron ionization spectra can be observed using time-resolved spectroscopy of photo-ionized electrons [21]. If the temporal resolution is not sufficient, only the steady-state parts $I^{\mathrm{st}}_0(E)$ and $I^{\mathrm{st}}_1(E)$ are experimentally available. We note that the Rabi oscillations can alternatively be observed in the long-time behavior of the two-level atom a provided that a suitable basis in the continuum of ionized states of atom b is chosen and a conditional measurement into its basis functions is considered.

The form of long-time spectra I^{lt}_0 and I^{lt}_1 as written in Eq. (18) guarantees that the overall long-time photoelectron ionization spectrum $I^{\mathrm{lt}}(E) = I^{\mathrm{lt}}_0(E,t) + I^{\mathrm{lt}}_1(E,t)$ is time independent;

$$I^{\mathrm{lt}}(E) = I^{\mathrm{st}}_0(E) + I^{\mathrm{st}}_1(E). \tag{18}$$

In the long-time photoelectron ionization spectra, there may occur frequencies that cannot be populated. If a given frequency E_F cannot be excited for arbitrary times, we have a Fano zero obeying the following equation:

$$I^{\mathrm{lt}}(E_F) = 0. \tag{19}$$

According to Eq. (18) a Fano zero at frequency E_F is present only if $I^{\mathrm{st}}_0(E_F) = 0$ and $I^{\mathrm{st}}_1(E_F) = 0$.

It may also happen that the long-time spectral components I^{st}_0, I^{st}_1, and I^{osc} fulfill one or both of the following equations for specific frequencies E_D:

$$I^{\mathrm{st}}_j(E_D) = I^{\mathrm{osc}}(E_D), \qquad j = 0,1. \tag{20}$$

This means that the long-time photoelectron ionization spectrum $I^{\mathrm{lt}}_0(E,t_D)$ [or $I^{\mathrm{lt}}_1(E,t_D)$] reaches zero at suitable time instants t_D. Such a frequency E_D corresponds to a dynamical zero that periodically occurs with the Rabi period $2\pi/\delta\xi$ [19]. We note that dynamical zeros occur because of the interaction of the autoionization system b with the two-level atom a. The frequencies of dynamical zeros depend, in general, on the state of the two-level atom a. However, if the two-level atom a is resonantly pumped, these frequencies in the long-time photoelectron spectra I^{lt}_0 and I^{lt}_1 coincide. We note that a Fano zero also obeys the conditions in Eq. (20) defining a dynamical zero.

III. PHOTOELECTRON IONIZATION SPECTRA

The long-time photoelectron ionization spectra of the Fano model as well as the ionization system interacting with a neighbor atom studied in [19] are useful in the analysis of spectra belonging to the autoionization system interacting with a neighbor. This is why we refer to them in the discussion below.

The general form of amplitude photoelectron ionization spectra $\mathbf{d}(E,t)$ of the interacting autoionization system is composed of eight Lorentzian curves, as Eqs. (12), (13), and (16) show. These curves are located at different frequencies E_r in the complex plane E. The complex frequencies E_r differ in the magnitudes of their complex parts and so they lead to peaks of different widths on the real axis E. In more detail, there exist two groups of four of the frequencies E_r (see Appendix A). The frequencies E_r in the second group are just those in the first group shifted by the Rabi frequency $\delta\xi$. However, as numerical results have revealed, only four frequencies E_r (two pairs) are important for the determination of shapes of the photoelectron ionization spectra I^{lt} in two regimes discussed here and assuming resonant pumping of atom a.

To demonstrate the main features found in the photoelectron ionization spectra, we first consider the comparable "ionization" interactions at atoms a and b ($V \approx J$, J_{ab}). The regime with $V \gg J$, J_{ab} appropriate for molecular condensates is analyzed subsequently.

Analyzing the long-time photoelectron ionization spectra, we first consider a weak direct ionization ($q_a, q_b \gg 1$; for definition of parameters, see the caption to Fig. 2). Upon assuming equally strong indirect ionization paths through states $|1\rangle_a$ and $|1\rangle_b$ ($q_a = q_b$), typical symmetric two-peak photoelectron ionization spectra are observed [see Fig. 2(a)]. We note that one should keep in mind that the ionization process through state $|1\rangle_a$ is not typical, since energy transfer without real transfer of electrons occurs. The greater the pumping parameter Ω is, the larger is the distance between two peaks that form an Autler-Townes doublet already discussed in the literature on autoionization processes (see, e.g., [8] and references therein). These conclusions can be drawn from the positions of eight frequencies E_r in the complex plane E discussed above. Their real parts are plotted in Fig. 3(a) as a function of the pumping parameter Ω. They create pairs with equal imaginary parts and mutual frequency difference equal to the Rabi frequency $\delta\xi$. Values of the imaginary parts of frequencies E_r indicate that only two pairs participate considerably in forming the long-time photoelectron spectra I^{lt}. Moreover, the frequencies E_r of these two pairs nearly coincide [see Fig. 3(a)]. This explains why the photoelectron ionization spectra I^{lt} are composed of only two peaks. We note that a two-peak structure is preserved even in the limit of weak optical pumping. The Fano-like zero at frequency $E = E_L$ can even be revealed for $\Omega \to 0$; see Sec. IV. This distinguishes the spectral profiles of the autoionization system compared to the Fano model (see Fig. 2(a) in [19]), having one central peak for weak optical pumping. Similarly to the Fano model, the peaks broaden with increasing pumping parameter Ω.

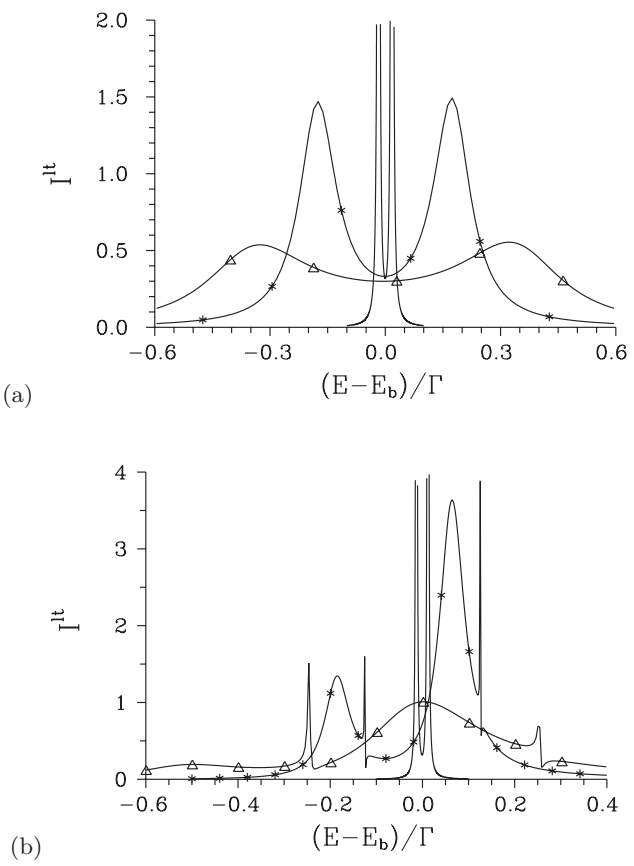

FIG. 2. Long-time photoelectron ionization spectra I^{lt} for (a) $q_a = q_b = 100$ and (b) $q_a = q_b = 1$ for different values of pumping parameter Ω: $\Omega = 0.1$ (solid curve), $\Omega = 1$ (solid curve with asterisks), and $\Omega = 2$ (solid curve with triangles). $\gamma_a = \gamma_b = 1$, $E_a = E_b = E_L = 1$, $J_{ab} = 0$; $q_a = \mu_a/(\pi\mu J^*)$, $\gamma_a = \pi|J|^2$, $q_b = \mu_b/(\pi\mu V^*)$, $\gamma_b = \pi|V|^2$, $\Omega = \sqrt{4\pi\Gamma(Q+i)\mu\alpha_L}$, $\Gamma = \gamma_a + \gamma_b$, and $Q = (\gamma_a q_a + \gamma_b q_b)/\Gamma$. Spectra are normalized such that $\int dE\, I^{\mathrm{lt}}(E) = 1$.

If the strength of a direct ionization path is comparable to those of two indirect ionization paths, the structure of long-time photoelectron ionization spectra is much richer [see Fig. 2(b)]. We can identify two sharp, nearly symmetrically positioned peaks in Fig. 2(b), with the mutual distance roughly given by the Rabi frequency $\delta\xi$. Contrary to the two symmetrically positioned peaks observed for large values of q_a, q_b in Fig. 2(a), the widths of these peaks practically do not depend on the pumping parameter Ω. Two additional, much broader peaks have been observed in the ionization spectra in Fig. 2(b) for larger values of pumping parameter Ω. The first peak can be found in the area around E_L; the second one occurs roughly one Rabi frequency $\delta\xi$ on the left-hand side of the first peak. If the pumping parameter Ω increases, the widths of both peaks and the distance between the peaks constituting the Autler-Townes doublet increases. Moreover, analysis of the behavior of eight complex frequencies E_r has shown that only two frequency pairs are located near the real axis of complex frequency E and thus build the spectrum I^{lt} [see Fig. 3(b)]. This explains why the peaks are mutually shifted by roughly one Rabi frequency. We note that the behavior of the second two peaks resembles that found for the two peaks in the long-time photoelectron spectrum of the ionization system interacting with a neighbor in [19] (compare Fig. 3(b) in [19]).

If indirect ionization including atom a prevails over the two remaining ionization channels, the long-time photoelectron ionization spectra are composed of two symmetrically positioned peaks. Moreover, the probability of ionization of the state with frequency E_a is practically zero [see Fig. 4(a)]. The greater the pumping parameter Ω is, the larger is the distance between two peaks and the peaks are broader. This behavior is qualitatively similar to that found for two side peaks in the

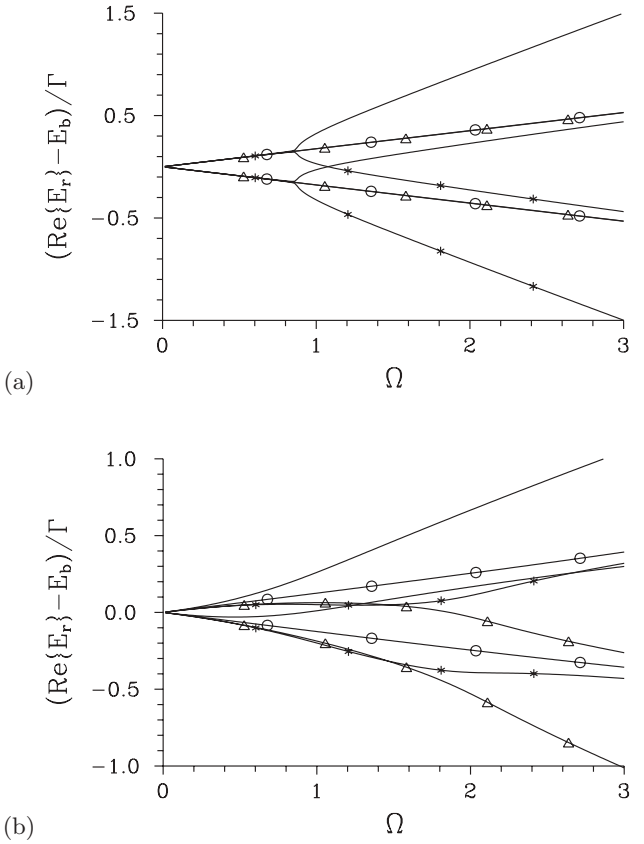

FIG. 3. Real parts of eight complex frequencies E_r, $E_r = \Lambda_{M^e,j} + \xi_k$ for $j = 1,\ldots,4$ and $k = 1,2$, indicating the positions of poles in spectra I^{lt} for (a) $q_a = q_b = 100$ and (b) $q_a = q_b = 1$ as they depend on pumping parameter Ω. Roots are divided into four pairs (plotted by different styles of curves) with equal imaginary parts and mutual frequency difference $\delta\xi$. Two pairs (solid curves with triangles and circles) have small imaginary parts and are thus visible in the spectra I^{lt} shown in Fig. 2. Values of other parameters are given in the caption to Fig. 2.

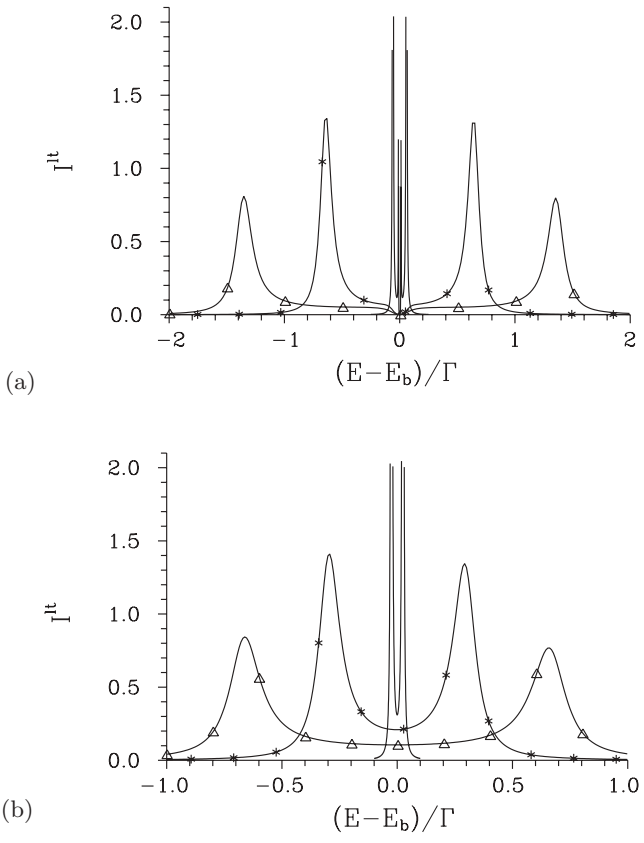

FIG. 4. Long-time photoelectron ionization spectra I^{lt} for (a) $q_a = 100$, $q_b = 1$ and (b) $q_a = 1$, $q_b = 100$ for different values of pumping parameter Ω: $\Omega = 0.1$ (solid curve), $\Omega = 1$ (solid curve with asterisks), and $\Omega = 2$ (solid curve with triangles). $\gamma_a = \gamma_b = 1$, $E_a = E_b = E_L = 1$, and $J_{ab} = 0$.

spectra of the ionization system interacting with a neighbor investigated in [19] (compare Fig. 2(b) in [19]). However, states with frequencies in the middle of the spectrum are only weakly occupied due to the interference with the additional ionization path coming through autoionizing state $|1\rangle_b$.

When the autoionization exploiting state $|1\rangle_b$ is dominant, Autler-Townes splitting of the photoelectron ionization spectrum [22] naturally occurs, as documented in Fig. 4(b). Even a weak indirect ionization based on the presence of neighbor atom a is sufficient to split the ionization peak typical of smaller values of the pumping parameter Ω into two symmetrically positioned side peaks. Symmetric two-peak photoelectron ionization spectra are thus observed independently of the value of pumping parameter Ω. The greater the pumping parameter Ω is, the more distant and broader are the peaks.

In molecular condensates, the dipole-dipole interaction between neighbor molecules has typical energies of 1–10 eV, whereas energies of electron volts characterize the Coulomb configuration interaction. The ratio γ_a/γ_b thus equals 10^{-4}–10^{-6} in this case. As the dipole-dipole interaction is weak ($\gamma_a \ll 1$), we are in the regime of $q_a \gg 1$ assuming comparable values of the dipole moments μ_a and μ. The role of state $|1\rangle_a$ in forming the photoelectron ionization spectra is important provided that the optical pumping dipole and dipole-dipole interactions have comparable strengths. This occurs only for weaker optical pumping. The needed pumping amplitudes α_L are thus lower by two or three orders of magnitude compared to those used in typical ionization experiments. An example of the dependence of the long-time photoelectron ionization spectra on the pumping parameter Ω is shown in Fig. 5. Figure 5(a) shows that the presence of molecule a leads to splitting of the spectral profile into two narrow peaks for smaller values of the pumping parameter Ω. The widths of these peaks broaden, their mutual distance increases, and their central frequencies shift toward lower frequencies as the values of the pumping parameter Ω increase. However, the peaks are gradually absorbed into an asymmetric spectral profile found for larger values of pumping parameter Ω [see Fig. 5(b)] and typical for the Fano model with one autoionization level in molecule b. The role of molecule a in the formation of ionization spectra is thus negligible for sufficiently large values of the pumping parameter Ω. In contrast, the interaction with molecule a substantially modifies the spectral profiles for smaller values of pumping parameter Ω, as comparison of curves in Fig. 5 and those in Fig. 3(a) in [19] clearly reveals.

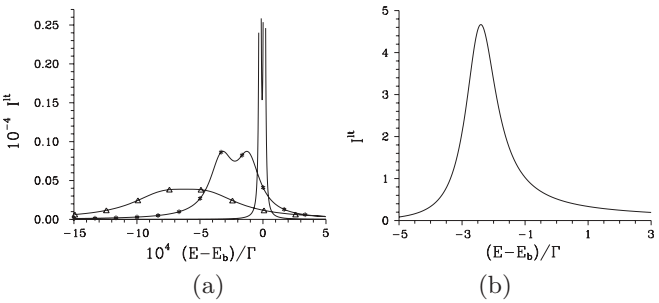

FIG. 5. Long-time photoelectron ionization spectra I^{lt} for (a) $\Omega = 0.5 \times 10^{-2}$ (solid curve), $\Omega = 3 \times 10^{-2}$ (solid curve with asterisks), $\Omega = 5 \times 10^{-2}$ (solid curve with triangles) and (b) $\Omega = 1$; $q_a = 100$, $\gamma_a = 1 \times 10^{-4}$, $q_b = \gamma_b = 1$, $E_a = E_b = E_L = 1$, and $J_{ab} = 0$.

Ionization spectra discussed up to now characterize the stationary long-time limit. Upon using the formulas given in Sec. II, temporal aspects of the formation of photoelectron ionization spectra can also be addressed. As the time t increases, the initially flat photoelectron ionization spectrum is gradually "focused" into its long-time shape. Naturally, the creation of sharper features in the long-time spectrum requires longer times, as illustrated in Fig. 6.

IV. FANO AND FANO-LIKE ZEROS IN LONG-TIME PHOTOELECTRON IONIZATION SPECTRA

Fano (Fano-like) and dynamical zeros are among the most important features of the long-time photoelectron ionization spectra. The form of these spectra built from up to eight Lorentzian curves [see Eqs. (12), (13), and (16)] allows us to draw general conclusions about the number of Fano and dynamical zeros (see Appendix B). It also allows us to develop a numerical method for finding frequencies of these zeros. According to this analysis, no more than three Fano zeros can exist.

Our investigations have revealed only one Fano zero (present for arbitrarily strong pumping) under specific conditions. In the limit of weak optical pumping, two Fano-like zeros have been identified.

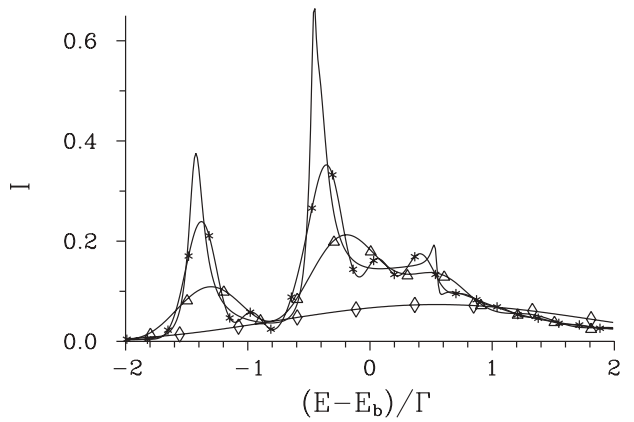

FIG. 6. Photoelectron ionization spectra I at different times t [$I(t) = I_0(t) + I_1(t)$]: $t = 1$ (solid curve with diamonds), $t = 5$ (solid curve with triangles), $t = 10$ (solid curve with asterisks), and $t \to \infty$ (solid curve). Spectrum I is determined as $I(E,t) = |d_0(E,t)|^2 + |d_1(E,t)|^2$; $q_a = q_b = \gamma_a = \gamma_b = 1$, $E_a = E_b = E_L = 1$, $J_{ab} = 0$, and $\Omega = 4$.

As for the Fano zero, its frequency E_F as well as the conditions for its observation can be revealed using a suitable canonical transformation [23]. From the physical point of view, this Fano zero may occur only provided that completely destructive interference between two ionization paths for atom b occurs as discovered in [1]. In our model, we have two additional ionization paths containing the energy transfer from the excited state $|1\rangle_a$ of atom a. In more detail, the first path contains direct energy transfer (J) into state $|E_F)$, whereas the second additional path includes energy transfer between states $|1\rangle_a$ and $|1\rangle_b$ (J_{ab}) and the Coulomb configurational interaction (V). These two additional ionization paths can also cancel each other under suitable conditions. A detailed analysis [23] has shown that state $|E_F)$ in the continuum is completely decoupled from both state $|0\rangle_b$ and state $|1\rangle_a$ only provided that [23]

$$\mu_b/\mu = J_{ab}/J. \tag{21}$$

The frequency E_F of the observed Fano zero is then given as $E_F = E_b - \gamma_b q_b$.

Two Fano-like zeros can be revealed in the limit of weak optical pumping, that is, when $\mu_a\alpha_L$, $\mu_b\alpha_L$, and $\mu\alpha_L$ are much lower than V and J. In this limit, the probability of having states $|1\rangle_a|1\rangle_b$ and $|1\rangle_a|E)$ describing two excited or ionized electrons is negligibly low compared to the other probabilities. A simplified scheme of states as shown in Fig. 7 can then be considered. This simplified model is suitable for the application of a canonical transformation [1] that gives two Fano-like zeros. This transformation "incorporates" states $|0\rangle_a|1\rangle_b$ and $|1\rangle_a|0\rangle_b$ into states $|E)$ of the continuum.

In this simplified scheme, we consider the Hamiltonian $\hat{H}_{ab}^{\mathrm{oneexc}}$, which quantifies the energy of states with one excited or ionized electron:

$$\begin{aligned}\hat{H}_{ab}^{\mathrm{oneexc}} = {} & E_a|1\rangle_{aa}\langle 1| + E_b|1\rangle_{bb}\langle 1| + \int dE\, E|E)(E| \\ & + [J_{ab}|1\rangle_{bb}\langle 0||0\rangle_{aa}\langle 1| + \mathrm{H.c.}] \\ & + \int dE\, [J|E)_b\langle 0||0\rangle_{aa}\langle 1| + \mathrm{H.c.}] \\ & + \int dE\, [V|E)_b\langle 1||0\rangle_{aa}\langle 0| + \mathrm{H.c.}]\,. \end{aligned} \tag{22}$$

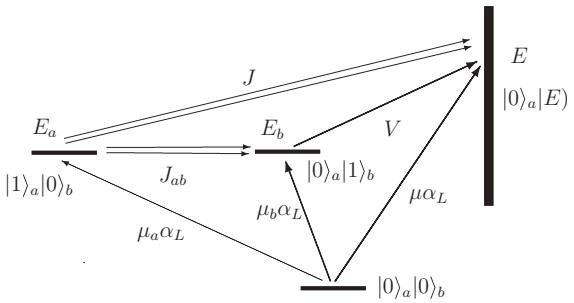

FIG. 7. Scheme of autoionization system b interacting with two-level atom a valid for negligible probabilities of states with two excited or ionized electrons. State $|0\rangle_a|0\rangle_b$ is the ground state; state $|0\rangle_a|1\rangle_b$ or $|1\rangle_a|0\rangle_b$ contains an excited electron at atom b or a, respectively; and state $|E)|0\rangle_a$ involves an ionized electron at atom b.

We need to find eigenstates of the Hamiltonian $\hat{H}_{ab}^{\text{oneexc}}$ and the corresponding dipole moments for the transitions from the ground state $|0\rangle_a|0\rangle_b$ into the states arising from the diagonalization. We note that the spectral long-time behavior of the system with Hamiltonian $\hat{H}_{ab}^{\text{oneexc}}$, Eq. (22), has been analyzed in [24] from the point of view of dc-field coupling of two autoionizing levels.

Eigenstates $|E)$ of the Hamiltonian $\hat{H}_{ab}^{\text{oneexc}}$ can be expressed as a linear superposition of states $|1\rangle_a|0\rangle_b$, $|0\rangle_a|1\rangle_b$, and $|0\rangle_a|E)$:

$$|E) = a(E)|1\rangle_a|0\rangle_b + b(E)|1\rangle_b|0\rangle_a + \int dE'\beta(E,E')|E')|0\rangle_a, \tag{23}$$

where $a(E)$, $b(E)$, and $\beta(E,E')$ are the coefficients of the superposition. They obey the following system of linear algebraic equations stemming from the stationary Schrödinger equation:

$$\begin{aligned} E_a a(E) + J_{ab}^* b(E) + \int dE' J^*(E')\beta(E,E') &= Ea(E), \\ J_{ab}a(E) + E_b b(E) + \int dE' V^*(E')\beta(E,E') &= Eb(E), \\ J(E')a(E) + V(E')b(E) + E'\beta(E,E') &= E\beta(E,E'). \end{aligned} \tag{24}$$

The third Eq. (24) can be solved in the following form:

$$\beta(E,E') = \frac{V(E')b(E) + J(E')a(E)}{E - E' + i\varepsilon} + F(E)\delta(E - E'), \tag{25}$$

where $\varepsilon > 0$ ($\varepsilon \to 0$ is assumed) and δ means the Dirac δ function. The coefficient $F(E)$ is determined from the normalization of state $|E)$. Substitution of the solution in Eq. (25) into the first two Eqs. (24) gives the set of coupled equations for the coefficients $a(E)$ and $b(E)$:

$$\begin{bmatrix} \tilde{E}_a - i\gamma_a - E & \tilde{J}_{ab}^* - i\pi J^*(E)V(E) \\ \tilde{J}_{ab} - i\pi J(E)V^*(E) & \tilde{E}_b - i\gamma_b - E \end{bmatrix} \times \begin{bmatrix} a(E) \\ b(E) \end{bmatrix} = -\begin{bmatrix} J^*(E)F(E) \\ V^*(E)F(E) \end{bmatrix}. \tag{26}$$

The damping constants γ_a and γ_b are given as $\gamma_a = \pi|J(E_0)|^2$ and $\gamma_b = \pi|V(E_0)|^2$ and the frequency E_0 lies in the center of the ionization spectrum. The renormalized frequencies $\tilde{E}_a$ and $\tilde{E}_b$ and the coupling constant $\tilde{J}_{ab}$ are determined along the expressions:

$$\begin{aligned} \tilde{E}_a(E) &= E_a + \mathcal{P}\int dE' \frac{|J(E')|^2}{E - E'}, \\ \tilde{E}_b(E) &= E_b + \mathcal{P}\int dE' \frac{|V(E')|^2}{E - E'}, \\ \tilde{J}_{ab}(E) &= J_{ab} + \mathcal{P}\int dE' \frac{J(E')V^*(E')}{E - E'}; \end{aligned} \tag{27}$$

$\mathcal{P}$ denotes the principal value. The solution of the two linear algebraic equations (26) can be found, for example, by finding the inverse matrix of the system. The normalization condition $|a(E)|^2 + |b(E)|^2 + \int dE'|\beta(E,E')|^2 = 1$ is fulfilled provided that we choose $F(E) = 1$. The coefficients $a(E)$, $b(E)$, and $\beta(E,E')$ can then be derived in their final form:

$$\begin{aligned} a(E) &= \frac{(E - \tilde{E}_b)J^*(E) + \tilde{J}_{ab}^* V^*(E)}{\mathcal{D}(E)}, \\ b(E) &= \frac{(E - \tilde{E}_a)V^*(E) + \tilde{J}_{ab} J^*(E)}{\mathcal{D}(E)}, \\ \beta(E,E') &= \frac{V(E')b(E) + J(E')a(E)}{E - E' + i\varepsilon} + \delta(E - E'). \end{aligned} \tag{28}$$

$\mathcal{D}(E)$ in Eq. (28) stands for the determinant of the matrix in Eq. (26), which is given as

$$\mathcal{D}(E) = (E - \tilde{E}_a)(E - \tilde{E}_b) + i\gamma_a(E - \tilde{E}_b) + i\gamma_b(E - \tilde{E}_a) - |\tilde{J}_{ab}|^2 + 2i\text{Re}\{t(E)\}. \tag{29}$$

In Eq. (29), $t(E) = \pi \tilde{J}_{ab}^* J(E)V^*(E)$. The function $t(E)$ is nonzero only if the energy transfer between excited state $|1\rangle_a$ and excited state $|1\rangle_b$ occurs.

The optical-field interaction between the ground state $|0\rangle_a|0\rangle_b$ and states with one excited or ionized electron as described by the Hamiltonian $\hat{H}_{ab}^{\text{oneexc}}$ is governed by the Hamiltonian $\hat{H}_{ab}^{\text{opt}}$:

$$\begin{aligned} \hat{H}_{ab}^{\text{opt}} = {} & [\mu_a\alpha_L \exp(-iE_L t)|1\rangle_{aa}\langle 0||0\rangle_{bb}\langle 0| + \text{H.c.}] \\ & + [\mu_b\alpha_L \exp(-iE_L t)|1\rangle_{bb}\langle 0||0\rangle_{aa}\langle 0| + \text{H.c.}] \\ & + \int dE\,[\mu\alpha_L \exp(-iE_L t)|E)_b\langle 0||0\rangle_{aa}\langle 0| + \text{H.c.}]. \end{aligned} \tag{30}$$

The Hamiltonian $\hat{H}_{ab}^{\text{opt}}$ transformed into the basis $|0\rangle_a|0\rangle_b$ and $|E)$ reads

$$\hat{H}_{ab}^{\text{opt}} = \int dE[\bar{\mu}(E)\alpha_L \exp(-iE_L t)|E)_a\langle 0|_b\langle 0| + \text{H.c.}]. \tag{31}$$

The dipole moment $\bar{\mu}$ in the transformed basis is given by the formula

$$\bar{\mu}(E) = \mu_a a^*(E) + \mu_b b^*(E) + \int dE'\mu(E')\beta^*(E,E'). \tag{32}$$

This formula can be recast in the following form:

$$\bar{\mu}(E) = \left[1 + \frac{(q_a + i)[\gamma_a(E - \tilde{E}_b) + t^*]}{\mathcal{D}^*(E)} + \frac{(q_b + i)[\gamma_b(E - \tilde{E}_a) + t]}{\mathcal{D}^*(E)}\right]\mu(E). \tag{33}$$

We recall that the parameters q_a and q_b are defined in the caption to Fig. 2.

The frequencies E_F giving the positions of Fano-like zeros can be easily identified using the condition $\bar{\mu}(E_F) = 0$ in Eq. (33). This leads to the quadratic equation

$$[E - \tilde{E}_b]^2 + [-\tilde{E}_a + \tilde{E}_b + q_a\gamma_a + q_b\gamma_b][E - \tilde{E}_b] + [q_a t^* + q_b(t - \gamma_b\tilde{E}_a + \gamma_b\tilde{E}_b) - |\tilde{J}_{ab}|^2] = 0. \tag{34}$$

The solution of quadratic equation (34) reveals the frequencies E_F of at most two Fano zeros:

$$[E_F]_{1,2} = \frac{\tilde{E}_a + \tilde{E}_b - q_a\gamma_a - q_b\gamma_b}{2} \pm \frac{\sqrt{D}}{2}. \qquad (35)$$

They occur for a non-negative discriminant D:

$$D = (\tilde{E}_a - \tilde{E}_b)^2 + (q_a\gamma_a + q_b\gamma_b)^2 - 2(\tilde{E}_a - \tilde{E}_b) \times (q_a\gamma_a - q_b\gamma_b) + 4|\tilde{J}_{ab}|^2 - 4q_a t^* - 4q_b t. \qquad (36)$$

We note that the frequencies E_F of two Fano zeros written in Eq. (36) coincide with those revealed in [7] for a double Fano system provided that $\tilde{J}_{ab} = 0$.

V. DYNAMICAL ZEROS IN LONG-TIME PHOTOELECTRON IONIZATION SPECTRA

The analysis reported in Appendix B reveals that up to 15 dynamical zeros can exist. Their frequencies E_D can be determined using the recipe described in Appendix B. We should note that the frequencies E_D of two of the dynamical zeros coincide with the frequencies E_F of the Fano-like zeros discussed in Sec. IV in the limit of weak optical pumping. If we plot the normalized frequencies $(E_D - E_b)/\Gamma$ of dynamical zeros as functions of the pumping parameter Ω, we arrive at graphs similar in shape to those appearing in the model of an ionization system interacting with a neighbor (see Fig. 6 in [19]). Graphs obtained for the analyzed model

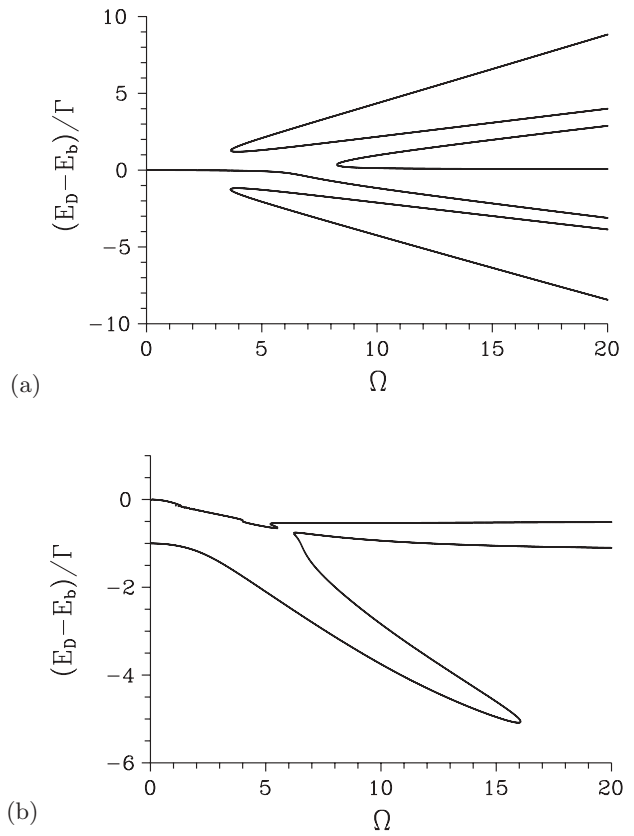

FIG. 8. Normalized frequencies $(E_D - E_b)/\Gamma$ of dynamical zeros as they depend on the pumping parameter Ω for resonant pumping of atom a: (a) $q_a = q_b = 100$, (b) $q_a = q_b = 1$. $\gamma_a = \gamma_b = 1$, $E_a = E_b = E_L = 1$, and $J_{ab} = 0$.

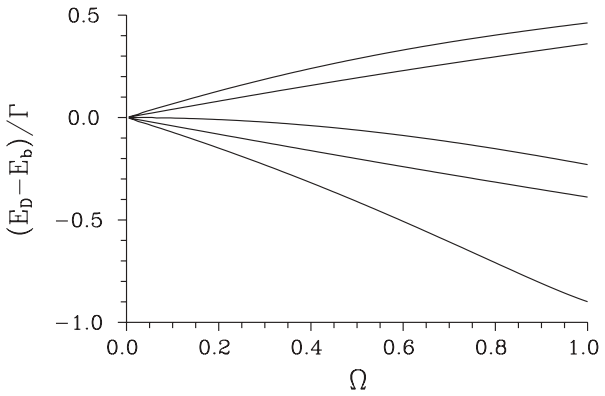

FIG. 9. Normalized frequencies $(E_D - E_b)/\Gamma$ of dynamical zeros as they depend on the pumping parameter Ω for resonant pumping of atom a: values of parameters are reported in the caption to Fig. 5.

are, in general, more complex. However, the creation and annihilation of dynamical zeros in pairs represent their most typical feature. As an example, graphs corresponding to the values of parameters defined in the caption to Fig. 2 are shown in Fig. 8. They demonstrate that the "creation" and "annihilation" of dynamical zeros occur in pairs. However, dynamical zeros can emerge in even greater numbers. This is documented in Fig. 9, where five dynamical zeros occur with frequency $E_D = E_b$ for $\Omega = 0$ for values of parameters typical for molecular condensates. Similarly to the long-time photoelectron ionization spectra of the ionization system interacting with a neighbor [19], splitting of the normalized frequencies $(E_D - E_b)/\Gamma$ appropriate to spectra I_0^{lt} and I_1^{lt} is observed for nonresonant pumping of the two-level atom a ($E_a \neq E_L$). The symmetry $\Omega \leftrightarrow -\Omega$ mentioned in [19] is also preserved in the analyzed autoionization system.

VI. CONCLUSIONS

The long-time photoelectron ionization spectra of an autoionization system interacting with a neighbor two-level atom have been investigated in several distinct regimes. They typically consist of several peaks with central positions and spectral widths depending on the pumping strength. As a consequence of the interference of several ionization paths, zeros occur in the long-time photoelectron ionization spectral profiles. Whereas only one genuine Fano zero has been found under special conditions, two Fano-like zeros observed only for weak optical pumping have been identified for a general system by constructing a suitable canonical transformation. The long-time photoelectron ionization spectra conditioned by the state of the neighbor two-level atom exhibit permanent Rabi oscillations. Spectral dynamical zeros observed once in the Rabi period have been revealed in these spectra. The frequencies of these dynamical zeros, depending on the strength of the optical pumping as well as the projected state of the neighbor two-level atom, have been analyzed.

ACKNOWLEDGMENTS

Support by Projects No. 1M06002 and COST OC 09026 and the Operational Program Research and

Development for Innovations–European Social Fund (Project No. CZ.1.05/2.1.00/03.0058) of the Ministry of Education of the Czech Republic as well as Project No. IAA100100713 of the GA AV ČR are acknowledged.

APPENDIX A: DETERMINATION OF POLES OF THE LORENTZIAN CURVES GIVING PHOTOELECTRON SPECTRA

The complex frequencies E_r giving poles of the Lorentzian curves composing photoelectron ionization spectra are determined as the sum of eigenvalues $\Lambda_{M^e,j}$ of the matrix $\mathbf{M^e}$ ($j = 1,\ldots,4$) and frequencies ξ_k ($k = 1,2$) giving Rabi oscillations of the two-level atom a, $E_r = \Lambda_{M^e,j} + \xi_k$. Whereas the frequencies ξ_k are written in Eq. (11), the eigenvalues $\Lambda_{M^e,j}$ can be derived from roots of the fourth-order polynomial written in the shifted frequency $\tilde{\Lambda}_{M^e}$; $\Lambda_{M^e} = \tilde{\Lambda}_{M^e} - i\pi|\mu\alpha_L|^2$:

$$[\tilde{\Lambda}_{M^e}]^4 + \alpha_3[\tilde{\Lambda}_{M^e}]^3 + \alpha_2[\tilde{\Lambda}_{M^e}]^2 + \alpha_1\tilde{\Lambda}_{M^e} + \alpha_0 = 0. \quad \text{(A1)}$$

The coefficients α_j introduced in Eq. (A1) can be derived from the elements of matrix $\mathbf{M^e}$:

$$\begin{aligned}
\alpha_0 &= (\Delta E_a + \mathcal{E}_b)\big[-\mathcal{E}_b M_a M_a^c + (-\Delta E_a + i\gamma_a)M_b M_b^c \\
&\quad + \big(M_a M_b^c j_{ab} + M_a^c M_b j_{ab}^c\big)\big]|\alpha_L|^2 + \big[M_a M_a^c|\mu_a|^2 \\
&\quad + M_b^2 M_b^{c2} - \big(M_a\mu_a^* + M_a^c\mu_a\big)M_b M_b^c\big]|\alpha_L|^4, \\
\alpha_1 &= (-\Delta E_a + i\gamma_a)(\Delta E_a + \mathcal{E}_b)\mathcal{E}_b + \big[(\Delta E_a - i\gamma_a)|\mu_a|^2 \\
&\quad + (\Delta E_a + 2\mathcal{E}_b)M_a M_a^c + (2\Delta E_a - i\gamma_a + 2\mathcal{E}_b) \\
&\quad \times M_b M_b^c\big]|\alpha_L|^2 + (\Delta E_a + \mathcal{E}_b)j_{ab}j_{ab}^c \\
&\quad - \big[(\mu_a + M_a)M_b^c j_{ab} + \big(\mu_a^* + M_a^c\big)M_b j_{ab}^c\big]|\alpha_L|^2, \\
\alpha_2 &= \Delta E_a(\Delta E_a - i\gamma_a) + (3\Delta E_a - 2i\gamma_a)\mathcal{E}_b + \mathcal{E}_b^2 \\
&\quad - \big[M_a M_a^c + |\mu_a|^2 + 2M_b M_b^c\big]|\alpha_L|^2 - j_{ab}j_{ab}^c, \\
\alpha_3 &= -2\Delta E_a - 2\mathcal{E}_b + i\gamma_a. \qquad \text{(A2)}
\end{aligned}$$

In Eq. (A2), $\mathcal{E}_b = \Delta E_b - i\gamma_b + i\pi|\mu\alpha_L|^2$, $M_a = \mu_a - i\pi\mu J^*$, $M_a^c = \mu_a^* - i\pi\mu^* J$, $M_b = \mu_b - i\pi\mu V^*$, $M_b^c = \mu_b^* - i\pi\mu^* V$, $j_{ab} = J_{ab} - i\pi J V^*$, and $j_{ab}^c = J_{ab}^* - i\pi J^* V$. Roots of the polynomial in Eq. (A1) can be found analytically, in principle, which might be useful in special cases.

APPENDIX B: DETERMINATION OF FANO AND DYNAMICAL ZEROS

The specific form of the long-time solution for the photoelectron spectra written in Eqs. (12), (13), and (16) allows us to reformulate the condition in Eq. (19) for the frequencies E_F of Fano zeros. They can be found as a common solution of the following four equations:

$$\sum_{j=1}^{4}\frac{A_j^{kl}}{E - \Lambda_{M^e,j} - \xi_l} = 0; \qquad k = 0,1, \quad l = 1,2. \quad \text{(B1)}$$

The coefficients A_j^{kl} can be derived from the solution in Eq. (13) as follows:

$$A_j^{kl} = [\mathbf{K_l B^{e\dagger} P^e}]_{kj}[\mathbf{P^{e-1}c}(0)]_j. \quad \text{(B2)}$$

Equations (B2) can be recast in the form of the third-order polynomials $p_{kl}(E)$,

$$p_{kl}(E) = \sum_{j=0}^{3}\alpha_j^{kl}E^j = 0, \quad \text{(B3)}$$

with the coefficients defined as

$$\begin{aligned}
\alpha_0^{kl} &= -\sum_{j=1}^{4}A_j^{kl}\prod_{m=1,m\neq j}^{4}(\Lambda_{M^e,m} + \xi_l), \\
\alpha_1^{kl} &= \sum_{j=1}^{4}A_j^{kl}\sum_{m=1,m\neq j}^{4}(\Lambda_{M^e,m} + \xi_l)\sum_{n=1,n\neq j,m}^{4}(\Lambda_{M^e,n} + \xi_l), \\
\alpha_2^{kl} &= -\sum_{j=1}^{4}A_j^{kl}\sum_{m=1,m\neq j}^{4}(\Lambda_{M^e,m} + \xi_l), \quad \alpha_3^{kl} = \sum_{j=1}^{4}A_j^{kl}. \qquad \text{(B4)}
\end{aligned}$$

A Fano zero is identified only provided that its frequency E_F is found simultaneously among three roots of the polynomials p_{kl} for all $k = 0,1$ and $l = 1,2$. Moreover, the corresponding root has to be real. In general, no more than three Fano zeros can be found.

The third-order polynomials p_{kl} introduced in Eq. (B3) are also useful in expressing the conditions $|d_k^{\xi_1}(E,t)| = |d_k^{\xi_2}(E,t)|$ [equivalent to those written in Eq. (20)] for the occurrence of dynamical zeros in the spectra I_k^{lt}, $k = 0,1$:

$$\begin{aligned}
&|p_{k1}(E)|\prod_{j=1}^{4}|E - \Lambda_{M^e,j} - \xi_2| \\
&\qquad = |p_{k2}(E)|\prod_{j=1}^{4}|E - \Lambda_{M^e,j} - \xi_1|, \qquad k = 0,1. \quad \text{(B5)}
\end{aligned}$$

Equation (B5) represents a 15th-order polynomial that can have complex coefficients. If the root of this polynomial is real, it gives the frequency E_D of a dynamical zero. In principle, up to 15 dynamical zeros might exist.

[1] U. Fano, Phys. Rev. **124**, 1866 (1961).
[2] K. Rzążewski and J. H. Eberly, Phys. Rev. Lett. **47**, 408 (1981).
[3] M. Lewenstein, J. W. Haus, and K. Rzążewski, Phys. Rev. Lett. **50**, 417 (1983).
[4] J. W. Haus, M. Lewenstein, and K. Rzążewski, Phys. Rev. A **28**, 2269 (1983).
[5] G. S. Agarwal, S. L. Haan, and J. Cooper, Phys. Rev. A **29**, 2552 (1984).
[6] K. Rzążewski and J. H. Eberly, Phys. Rev. A **27**, 2026 (1983).

[7] W. Leoński, R. Tanaś, and S. Kielich, J. Opt. Soc. Am. B **4**, 72 (1987).
[8] W. Leoński and R. Tanaś, J. Phys. B **21**, 2835 (1988).
[9] P. Lambropoulos and P. Zoller, Phys. Rev. A **24**, 379 (1981).
[10] L. Journel, B. Rouvellou, D. Cubaynes, J. M. Bizau, F. J. Willeumier, M. Richter, P. Sladeczek, K.-H. Selbman, P. Zimmerman, and H. Bergerow, J. Phys. IV **3**, 217 (1993).
[11] E. Paspalakis, N. J. Kylstra, and P. L. Knight, Phys. Rev. A **60**, 642 (1999).
[12] A. Raczyński, M. Rzepecka, J. Zaremba, and S. Zielińska-Kaniasty, Opt. Commun. **266**, 552 (2006).
[13] M. Lewenstein and K. Rzażewski, Phys. Rev. A **61**, 022105 (2000).
[14] W. Leoński and V. Bužek, J. Mod. Opt. **37**, 1923 (1990).
[15] W. Leoński, J. Opt. Soc. Am. B **10**, 244 (1993).
[16] P. Durand, I. Paidarová, and F. X. Gadéa, J. Phys. B **34**, 1953 (2001).
[17] A. E. Miroshnichenko, S. Flach, and Y. S. Kivshar, Rev. Mod. Phys. **82**, 2257 (2010).
[18] W. Leoński, R. Tanaś, and S. Kielich, J. Phys. D **21**, S125 (1988).
[19] J. Peřina Jr., A. Lukš, W. Leoński, and V. Peřinová, Phys. Rev. A, in press (2011).
[20] E. A. Silinsh and V. Čápek, *Organic Molecular Crystals: Interaction, Localization and Transport Phenomena* (Oxford University Press/American Institute of Physics, Melville, NY, 1994).
[21] P. Meystre and P. Sargent III, *Elements of Quantum Optics* (Springer, Berlin, 2007).
[22] S. H. Autler and C. H. Townes, Phys. Rev. **100**, 703 (1955).
[23] A. Lukš, V. Peřinová, J. Peřina Jr., J. Křepelka, and W. Leoński, in *Wave and Quantum Aspects of Contemporary Optics: Proceedings of SPIE*, edited by J. Müllerová, D. Senderáková, and S. Jurecka, Vol. 7746 (SPIE, Bellingham, WA, 2010), p. 77460W.
[24] W. Leoński and R. Tanaś, J. Opt. Soc. Am. B **8**, 6 (1991).